The dynamic enhanced characterization with low mechanical index gray-scale harmonic imaging inflammatory pseudotumor of liver compared with hepatic VX2 tumor and normal liver

Ying Shi[A–F], Xinghua Wang[A,E], Yingyan Qiao[B,C], Xueping Bai[B,C], Qinxiu Wang[B], Chenggong Lei[C]

Department of Ultrasound, Second Hospital of Shanxi Medical University, Taiyuan, China

A – research concept and design; B – collection and/or assembly of data; C – data analysis and interpretation;
D – writing the article; E – critical revision of the article; F – final approval of the article

Advances in Clinical and Experimental Medicine, ISSN 1899–5276 (print), ISSN 2451–2680 (online) *Adv Clin Exp Med*. 2020;29(9):1073–1081

Address for correspondence
Xinghua Wang
E-mail: wang_xh1972@sina.com

Funding sources
This research project was supported by Shanxi Scholarship Council of China (grant No. 2013-058), Nature Science Foundation of Shanxi Province (grant No. 201801D121323) and Doctor Start-up Fund of Shanxi Medical University, Taiyuan, China (grant No. BS201716).

Conflict of interest
None declared

Received on January 24, 2018
Reviewed on September 17, 2018
Accepted on June 27, 2019

Published online on September 4, 2020

Abstract

Background. Inflammatory pseudotumor of the liver (IPTL) is misdiagnosed usually as a malignant tumor based on the imaging findings. Differential diagnosis should be established to avoid hepatic resection. At imaging, IPTL has been misdiagnosed usually as hepatocellular carcinoma (HCC). It is usually found firstly using conventional ultrasonic examination, which cannot give a definitive diagnosis. Because of its atypical clinical presentation and radiological appearance, a presumptive diagnosis of malignancy is frequently made. With the development of ultrasound systems and ultrasound contrast agents (UCA), contrast-enhanced ultrasound is widely used in diagnosing focal lesions of the liver.

Objectives. To delineate the hemodynamic features of IPTL compared with hepatic VX2 tumor and normal liver using contrast-enhanced ultrasound.

Material and methods. Freund's complete adjuvant (FCA) was injected using a modified method into the desirable portion of the liver in rabbits. Two weeks after the injection, solitary IPTLs were formed (which was proved with pathological examination). Ten rabbits with IPTL, 10 rabbits with VX2 carcinoma and 10 healthy rabbits were studied using contrast-enhanced ultrasound with bolus injection of SonoVueTM through the peripheral vein. Corresponding parameters such as time to enhancement (ET), time to peak intensity (PIT), time to ascent (AT), and time to lighten (LT) were measured with wash-in/wash-out curve.

Results. Contrast-enhanced imaging clearly delineated the dynamic enhancement of the lesions and liver parenchyma during the whole phase. Inflammatory pseudotumor of the liver showed the same enhanced features as the liver parenchyma. In VX2 tumors, hyperechoic enhancement in arterial phase and hypoechoic enhancement was observed in the portal and delayed phase compared with the surrounding hepatic parenchyma. The normal liver showed whole of liver parenchyma enhanced in portal phase.

Conclusions. The study showed that contrast-enhanced ultrasound provided useful information about perfusion in IPTL and VX2 carcinoma. Contrast-enhanced ultrasound is a useful technique in the differential diagnosis of focal liver lesions if combined with time-intensity curve.

Key words: liver, ultrasonography, inflammatory pseudotumor, contrast agent, ultrasonic diagnosis

Cite as
Shi Y, Wang X, Qiao Y, Bai X, Wang Q, Lei C. The dynamic enhanced characterization with low mechanical index gray-scale harmonic imaging inflammatory pseudotumor of liver compared with hepatic VX2 tumor and normal liver. *Adv Clin Exp Med*. 2020;29(9):1073–1081. doi:10.17219/acem/110315

DOI
10.17219/acem/110315

Introduction

Inflammatory pseudotumor of the liver (IPTL) is a benign, tumor-like mass, which was first described in 1953 by Pack and Baker.[1] The lesion is characterized by encapsulated proliferating connective tissue admixed with inflammatory cells.[2] Clinical presentation and morphological appearance may vary.[3] It is difficult to arrive at a definitive diagnosis in the absence of a clinical abnormality.[4] Inflammatory pseudotumor of the liver is misdiagnosed usually as a malignant tumor based on the imaging findings.[5–7] The diagnosis in most cases was confirmed during surgery and biopsy.[8] Differential diagnosis should be established to avoid hepatic resection.[9]

At imaging, IPTL has been misdiagnosed usually as hepatocellular carcinoma (HCC). Inflammatory pseudotumor of the liver is usually found with conventional ultrasonic examination, which cannot give the definitive diagnosis. Further examination, such as contrast-enhanced computed tomography (CT) and contrast-enhanced magnetic resonance imaging (MRI), needs to be undertaken. However, sonographic enhancement demonstrates a variable pattern of echogenicity. The lesion has been documented as hypo- or hyperechogenic, with or without mosaic pattern, and with ill-defined or well-circumscribed margins.[4,10] Because of its atypical clinical presentation and radiological appearance, a presumptive diagnosis of malignancy is frequently made.

With the development of ultrasound systems and ultrasound contrast agents (UCA), contrast-enhanced ultrasound is widely used in diagnosing focal lesions of the liver.[11,12] The perfusion of lesions is assessed with gray-scale harmonic imaging at a low mechanical index (MI) level. Dynamic changes of contrast enhancement in the liver tumor are observed using real-time continuous gray-scale imaging. Furthermore, quantitative assessment of circulation in liver is achieved with the time-intensity-curve software, which obtains different curves indicating tissue and vascular uptake, transit times, and wash-out of the contrast agent.[13–17]

Therefore, we performed a pilot study to establish an animal model carrying IPTL in rabbits with Freund's complete adjuvant (FCA) serving for contrast-enhanced ultrasound, and to explore the dynamic enhancement characterization of the IPTL compared with hepatic VX2 tumor, surrounding parenchyma and normal liver. Corresponding parameters such as time to enhancement (ET), time to peak intensity (PIT), time to ascent (AT), and time to lighten (LT) were measured with a time-intensity curve to evaluate the potential usefulness of quantifing perfusions in focal liver lesions.

Material and methods

Animal model

Twenty male rabbits, weighing 1.8–2.5 kg (mean body weight: 2.2 kg) with healthy livers, were divided into 3 groups (A, B and C). Group A was the IPTL group (included 10 rabbits), group B the VX2 hepatic tumor group (10 rabbits), and group C the healthy control group (10 rabbits).

Establishment of hepatic inflammatory pseudotumor modified model

Ten rabbits were anesthetized with Sumianxin (Changchun Argo-Pastoral University, Jilin, China), which does not affect the cardiovascular system, at a dose of 1.5 mg/kg bw. through an intramuscular injection. The rabbits were placed in a supine position after the skin of the abdomen was shaved with 8% sodium sulfide solutions. Using a sterile technique, a small subxyphoid midline incision was made. In the test experiment, FCA (containing tuberculin, steroid, protein, and polysaccharide) was directly injected into the lobe of the liver in 10 rabbits according to the recorded method.[18] However, histopathological examination proved that no focal lesions formed in the place of large size areas with diffuse necrosis. Then, we modified the method and inserted 1 mm^3 of gelfoam into the left and right liver lobes with ophthalmic forceps through laparotomy incisions. Next, FCA was injected slowly into the gelfoam. The incision hole was pressed for 2–3 min after pulling out the syringe so FCA did not flow out from the needle tunnel. The sonographic study was conducted 2 weeks after the implantations.

Establishment of hepatic VX2 tumor model

Ten rabbits were prepared as IPTL group. A small subxyphoid midline incision was made and about 1 mm^3 of tumor tissue from a carrier rabbit was inserted into the left and right liver with ophthalmic forceps under direct observation. The sonographic study was conducted 2 weeks after the implantation.

The rabbits were sacrificed after the sonographic study, and histopathological examinations were performed. The studies were conducted in compliance with the regulations of the Animal Ethics Committee of Shanxi Medical University, Taiyuan, China.

Contrast agents and administration

The contrast agent used in the study was SonoVue™ (Bracco SpA, Milan, Italy), which is a lipid-shelled ultrasound contrast agent that contains millions of microbubbles filled with sulphur hexafluoride gas. A white, milky suspension of microbubbles was obtained by adding 5 mL of physiologic saline (0.9% sodium chloride) to the powder (25 mg) with the use of standard clinical aseptic techniques, followed by hand agitation. The injection of SonoVue™ was administered through a 26-gauge catheter placed into a marginal ear vein, followed by 2 mL of saline flush. SonoVue™ at a dose of 0.1 mL/kg bw. was applied.

Equipment and data analysis

Fundamental gray-scale imaging and contrast-tuned imaging (CnTI) were conducted using a Technos MPX DU8 ultrasonography system (Esaote Biomedical SpA, Genoa, Italy). A broad-band linear array transducer, operating at 8–3 MHz for fundamental imaging and 1.56 MHz for CnTI, was used. The scanning settings for the optimal visualization, including the gain, scanning depth, field of view, and time gain control, were determined from a test experiment in several rabbits and remained unchanged throughout this study. The rabbits were scanned using conventional ultrasound to observe the lesions and normal liver (the left and right liver lobe), recording the location, the size, the features of the echogenicity, and the color flowing characterization before injecting the contrast agent. The probe was fixed during the whole period of contrast-enhanced examination when determining the optimal imaging plane showing the lesions surrounding parenchyma or normal liver each the left and right liver lobe. Then CnTI was triggered with a low MI of 0.106. After each UCA injection, digitized gray-scale images of the liver in situ within 2 min were stored in a continuous loop review and recorded on a built-in hard disk for off-line analysis.

For the analysis of gray-scale parameters, the digitally stored data of the lesions surrounding parenchyma and normal liver, were measured offline with wash-in/wash-out software built into the Technos^{MPX} DU8 system. The regions of interest (ROI) of the same shape and size were set in liver lesions surrounding parenchyma and normal liver, each the left and right liver lobe, in approximately the same depth. The ROI were established in the center and/or the enhanced rim of the lesions. Corresponding parameters including time to enhancement (ET), time to peak intensity (PIT), time to ascent (AT), and time to lighten (LT) were measured using a time-intensity curve. The ET was defined as the delay from injection until the first echogenic bubbles of contrast agent could be seen. The PIT was defined as the interval from the beginning of the injection to the peak of the time-intensity curve. The AT was the interval calculated as PIT minus ET. The LT was defined as the interval from the injection to wash-out platform of the time-intensity curve after the enhancement peak.

Statistical analyses

Data was expressed as means and standard deviations (SD). The ET, PIT, AT, and LT of liver lesions and surrounding parenchyma in IPTL group and VX2 tumor group for each imaging protocol were compared using a paired two-tailed Student's t-test. The ET, PIT, AT, and LT for each imaging protocol were compared with a one-way analysis of variance (ANOVA) among IPTL group, VX2 tumor group and the normal liver group, and post hoc tests of pairwise comparison were used for comparisons between the 3 groups. Differences were considered significant at $p < 0.05$. The software used was SPSS v. 11.5 (SPSS Inc., Chicago, USA).

Results

Pathology results

IPTL group

Twenty lesions were implanted in 10 rabbits and 17 nodules (range: 4.6–13.8 mm) were formed successfully. The incidence rate is 85%. Gross appearance showed white, round and solid nodules with definite capsules (Fig. 1A). Microscopically, the nodule showed marked fibrosis with infiltration of mixed population of inflammatory cells and multinucleate cells (Fig. 1B). The middle zone was proliferated granulomatous tissue and fibrous tissue. Degenerated liver tissue was seen in the center of the nodule. Scattered necrosis, diffused fat and amorphous substance were also present. Obvious inflammatory reaction and fibrous tissue were observed at the periphery of the lesions. More venous vessels than arteries were seen in the peripheral zone of the lesion. Degeneration and necrosis were observable in most of tiny arteries.

VX2 tumor group

Twenty lesions were implanted in 10 rabbits and 19 nodules (range: 4.2–15.3 mm) were formed successfully. Gross appearance showed grayish-white, hard and round nodules (Fig. 1C) whose borders were well-circumscribed but not encapsulated. Microscopically, the tumor showed scattered cancer nests infiltrating the liver tissues (Fig. 1D). The tumor nests consisted of large polygonal cells with many mitotic figures. Disorder hepatic cord and dilated small vessels were present around the cancer nests. There were abundant newborn capillaries, in some of which tumor emboli were observed.

Healthy control group

Twenty liver lobes (both left and right liver lobe of each 10 healthy rabbits) were collected. Each liver lobe was red and had no nodules (Fig. 1E). Microscopically, the liver lobes had hepatocytes with normal architecture and observable sinusoids (Fig. 1F).

On-site observation and offline assessment

Low-MI gray-scale imaging clearly delineated the dynamic enhancement of the lesions and parenchyma during the whole phase. The comparison of the on-site enhancement between IPTL VX2 tumors and normal livers is shown in Table 1. The time-intensity curves were analyzed during the phases of acquisition time (wash-in) and release of the contrast agent (wash-out), in addition to the evaluation of the shape of the resulting curve.

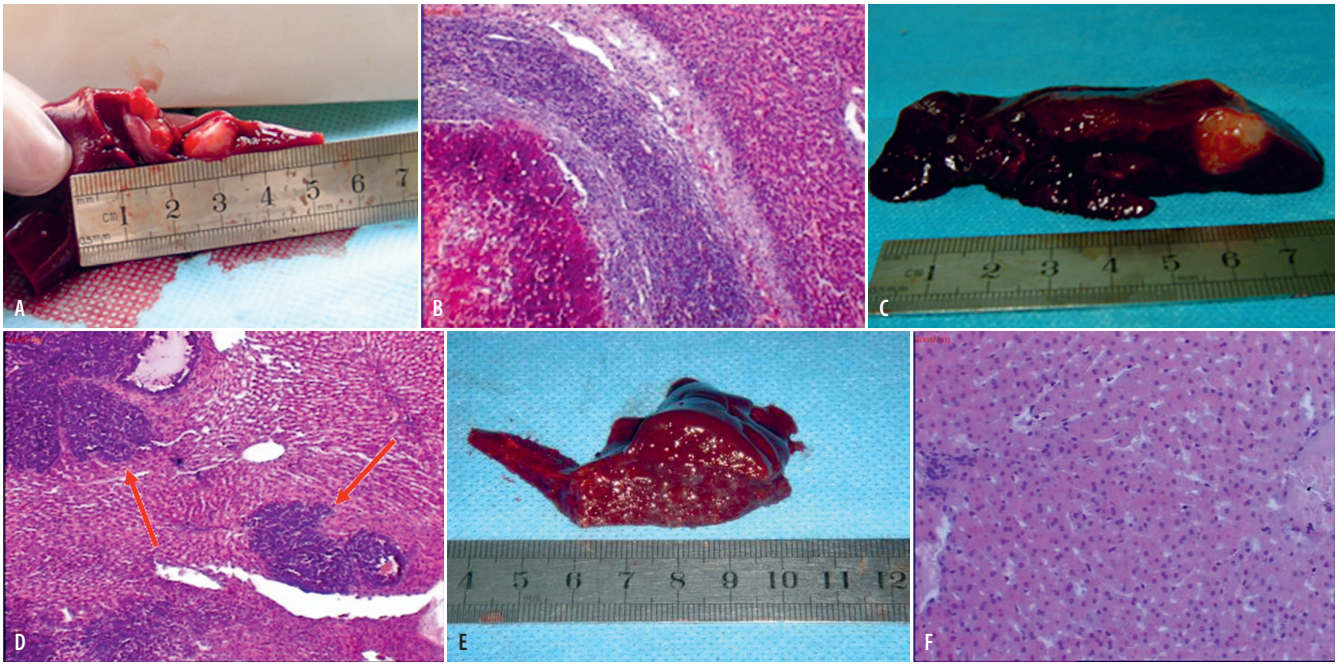

Fig. 1. Pathology results. A – IPTL group. Photography of gross appearance showing white, round and solid nodules with definite capsule. B – IPTL group. Photomicrograph showing marked fibrosis with infiltration of mixed population of inflammatory and multinucleate cells (H&E staining, magnification ×100). C – VX2 tumor group. Photography of gross appearance showing grayish-white mass well-circumscribed with no definite capsules. D – photomicrograph showing scattered cancer nests infiltrated among the liver tissues (red arrow) (H&E staining, magnification ×100). E – normal liver group. Photography of gross appearance showed red and homogeneous liver, without nodes. F – normal liver group. Photomicrograph showing normal liver lobe had hepatocytes with normal architecture and observable sinusoids (H&E staining, magnification ×400)

Table 1. The enhancement in IPTL and VX2 tumors in whole phase

Group	Arterial phase	Portal phase	Delayed phase
IPTL	same as parenchyma	no dark areas	no dark areas
VX2 tumor	marked enhanced	decreased enhancement	marked dark areas
Normal liver	enhanced hepatic artery	enhanced liver parenchyma	delayed liver parenchyma

ITPL – inflammatory pseudotumor of the liver.

Table 2. The comparison of ET, PIT, AT, and LT between IPTL and parenchyma

Group	ET [s]	PIT [s]	AT [s]	LT [s]
IPTL	10.46 ±2.05	30.35 ±9.81	17.93 ±8.03	80.59 ±25.68
Parenchyma	10.84 ±2.46	27.43 ±9.27	16.59 ±8.73	77.95 ±25.68
p-value	0.653	0.199	0.526	0.655

Values are presented as means ± standard deviation (SD); ITPL – inflammatory pseudotumor of the liver; ET – time to enhancement; PIT – time to peak intensity; AT – time to ascent; LT – time to lighten.

IPTL group

Ordinary ultrasound scanning showed iso- or hyperechoic nodules of IPTL (Fig. 2A), which revealed an absence of color flow before the injection of UCA (Fig. 2B). After the injection of UCA, IPTL showed the same enhanced features and dynamic changes as that of liver parenchyma during the whole enhanced phase. The enhancement of all nodules was no greater than that of parenchyma in arterial phase (Fig. 2C). Hypoechoic nodules were not observed in portal phase and delayed phase compared with parenchyma (Fig. 2D). The curves obtained from the IPLT and parenchyma had similar patterns, showing a regular progressive wash-in and slowly wash-out of the UCA (Fig. 2E,F). The ET, PIT, AT, and LT in IPTL were 10.46 ±2.05 s, 30.35 ±9.81 s, 17.93 ±8.03 s, and 80.59 ±25.68 s, respectively. The ET, PIT, AT, and LT in parenchyma of IPTL were 10.84 ±2.46 s, 27.43 ±9.27 s, 16.59 ±8.73 s, and 77.95 ±25.68 s, respectively. There was no significant difference for ET, PIT, AT, and LT between IPTL and parenchyma ($p > 0.05$) (Table 2).

VX2 tumor group

Ordinary ultrasound scanning revealed that the VX2 tumors showed hypo-, iso- or hyperechoic imaging (Fig. 3A).

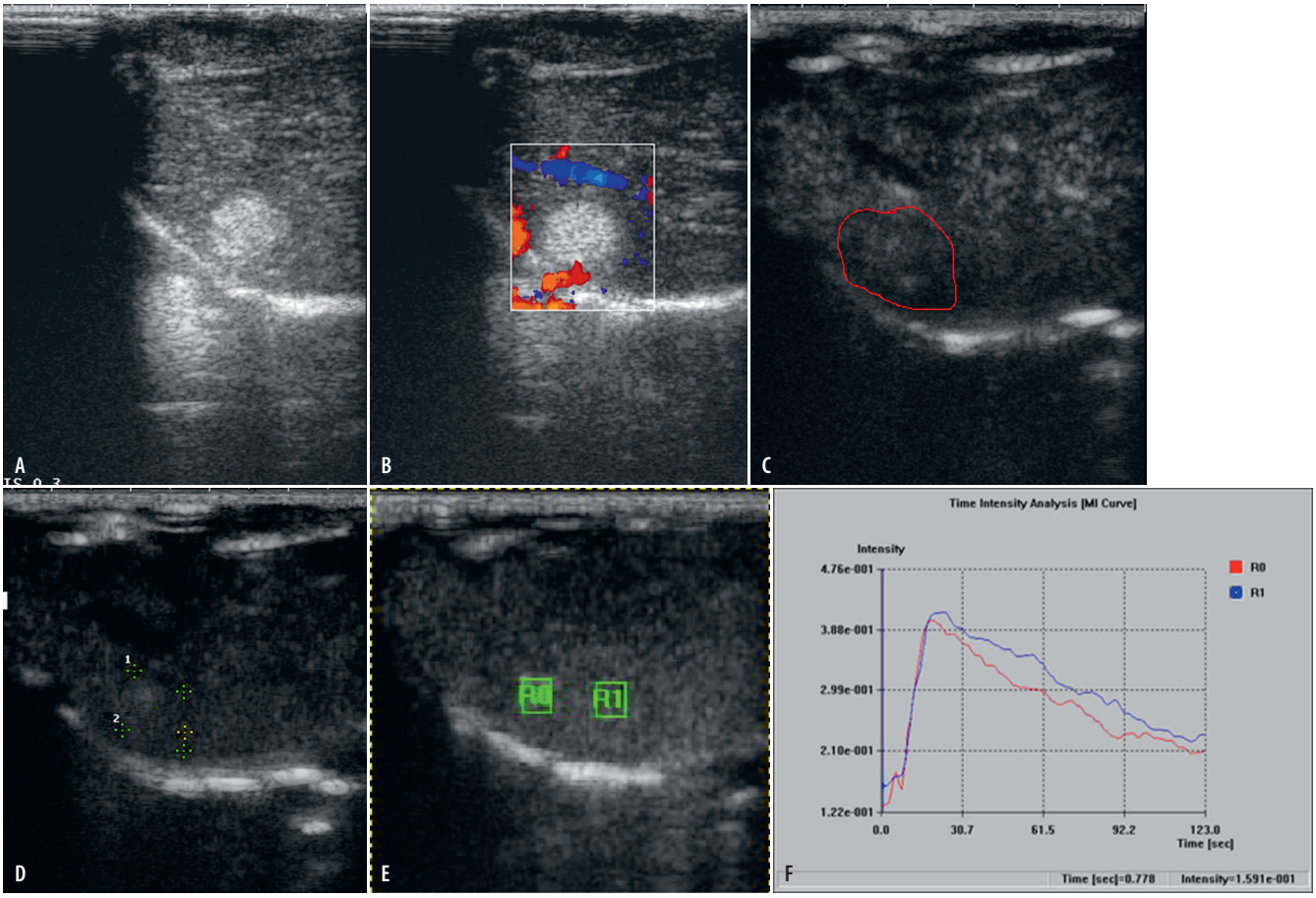

Fig. 2. IPTL group. A – hyperechoic nodule in conventional ultrasound imaging; B – no blood flow in color Doppler flow imaging; C – enhancement in the arterial phase, no marked enhanced change compared with the parenchyma (red circle); D – enhanced feature same as the parenchyma in delayed phase; E – the ROI were set in the center of the lesion (R0) and parenchyma (R1) in approximately the same depth; F – the curves obtained from the IPTL and parenchyma had similar patterns and showed a regular progressive wash-in and slowly wash-out of the UCA (red curve – IPTL; blue curve – parenchyma)

Noise signal was seen in 9 tumors (Fig. 3B) and artery signal was observed in 4 tumors. After the UCA injection, the tumors were enhanced markedly in the early arterial phase (Fig. 3C). The features of the enhancement in the early arterial phase showed 3 patterns: enhancement on the rim of the tumors (7 nodules), homogeneous enhancement of the whole tumors (2 nodules) and heterogeneous enhancement of the tumors (4 nodules). The tumors were clearly and easily identified as areas of enhancement because the parenchyma was just slightly enhanced in the early arterial phase. After the arterial phase, the echogenicity of the surrounding liver tissue increased, and the intensity of the tumors decreased gradually before falling off abruptly. The UCA was washed out earlier from tumors than from parenchyma. The tumors were clearly identified as dark areas compared with the enhanced parenchyma in portal (Fig. 3D) and delayed phases.

Results obtained in the VX2 tumor and liver parenchyma

The curves obtained from the VX2 tumors had different patterns from those obtained from the surrounding live parenchyma. The curve obtained in VX2 tumors displayed abruptly rapid wash-in curve and returned much earlier than the parenchyma to the baseline (Fig. 3E,F). The ET, PIT, AT, and LT in VX2 tumor were 7.59 ±1.58 s, 22.47 ±7.16 s, 14.75 ±7.37 s, and 34.47 ±13.15 s, respectively. The ET, PIT, AT, and LT in parenchyma of VX2-tumor bearing rabbits were 10.02 ±2.74 s, 32.53 ±12.07 s, 22.60 ±11.51 s, and 81.84 ±23.55 s, respectively. The ET, PIT, AT and LT in VX2 tumors were significantly ($p < 0.05$) shorter than those of the live parenchyma (Table 3).

Healthy control group

Ordinary ultrasound scanning revealed that the normal liver lobes showed homogeneous isoechoic imaging (Fig. 4A), which had normal color flow before the injection of UCA (Fig. 4B). After the injection of UCA, the liver lobes showed only hepatic artery enhanced in the arterial phase (Fig. 4C), while later the whole liver parenchyma was enhanced in portal phase (Fig. 4D) and decayed in delayed phase. The curves obtained from the normal liver parenchyma showed a regular progressive wash-in and slow wash-out of the UCA. The ET,

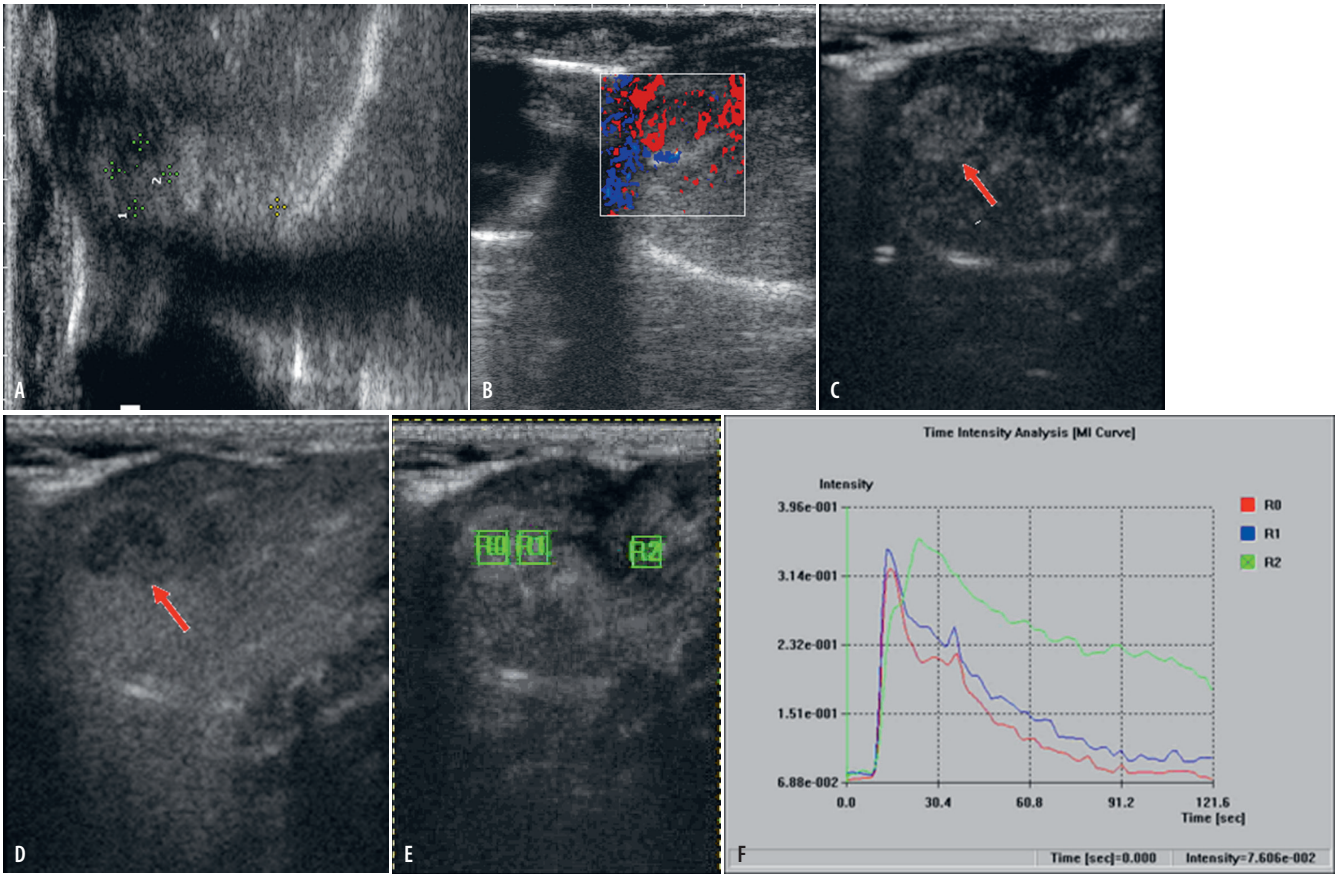

Fig. 3. VX2 tumor group. A – hypoechoic nodule with ill-definite in conventional ultrasound imaging; B – no blood flow instead of noise in color Doppler flow imaging; C – marked enhancement (red arrow) in the arterial phase compared with the parenchyma; D – wash-out UCA and dark lesion in portal phase (red arrow); E – the ROI were set in the center of the lesion (R0), the rim of lesion (R1) and parenchyma (R2) in approximately the same depth; F – the curves displayed abruptly rapid wash-in curve and returned much earlier than the parenchyma to the baseline (red curve – the center of VX2 tumor, blue curve – the rim of VX2 tumor, green curve – parenchyma)

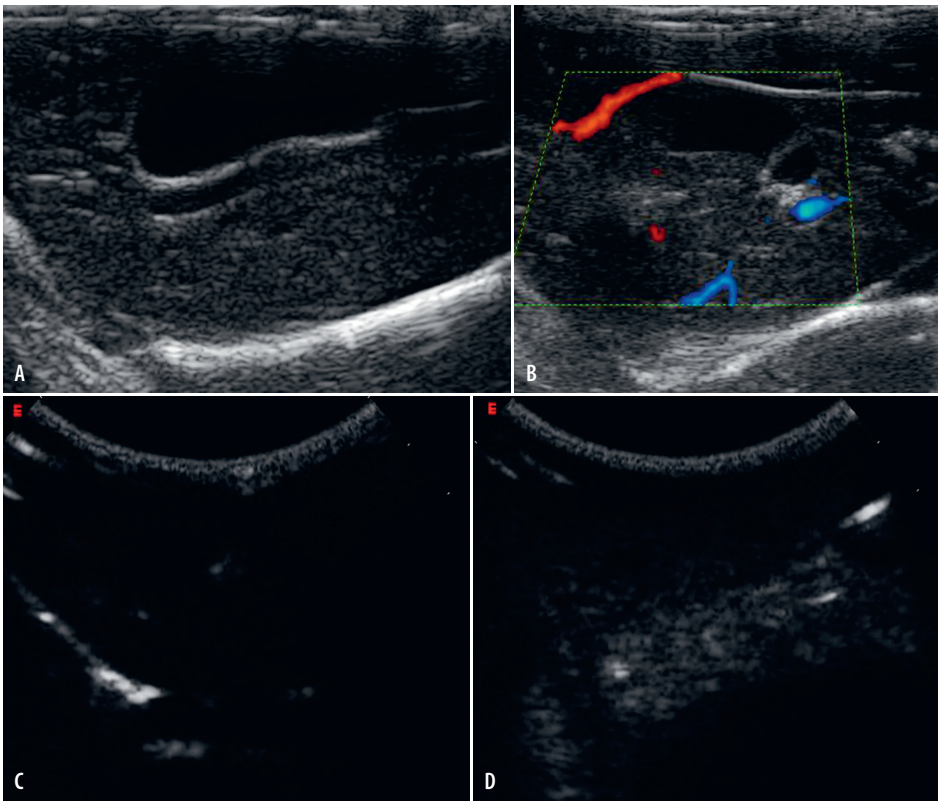

Fig. 4. Normal liver group. A – the normal liver lobes showing homogeneous isoechoic imaging; B – normal shape of color flow in color Doppler flow imaging; C – the liver lobes showing only hepatic artery enhanced in the arterial phase; D – whole liver parenchyma enhanced in portal phase

Table 3. The comparison of ET, PIT, AT, and LT between VX2 tumors and parenchyma

Group	ET(s)	PIT(s)	AT(s)	LT(s)
VX2	7.59 ±1.58	22.47 ±7.16	14.75 ±7.37	34.47 ±13.15
Parenchyma	10.02 ±2.74	32.53 ±12.07	22.60 ±11.51	81.84 ±23.55
p-value	0.006*	0.009*	0.038*	0.000*

Values are presented as means ± standard deviation (SD); * $p < 0.05$. ET – time to enhancement; PIT – time to peak intensity; AT – time to ascent; LT – time to lighten.

Table 4. The comparison of ET, PIT, AT, and LT among IPTL and VX2 tumors and normal liver

Group	ET(s)	PIT(s)	AT(s)	LT(s)
IPTL	10.46 ±2.05#	30.35 ±9.81#	17.93 ±8.03	80.59 ±25.68#
VX2	7.59 ±1.58*	22.47 ±7.06*	14.75 ±7.37	34.47 ±13.15*
Normal liver	10.16 ±1.76#	29.18 ±9.99#	18.30 ±6.67	79.00 ±16.87#

Values are presented as means ± standard deviation (SD); * value is significantly different from the IPTL group value, # $p < 0.05$; # value is significantly different from the VX2 tumor group value, # $p < 0.05$. ITPL – inflammatory pseudotumor of the liver; ET – time to enhancement; PIT – time to peak intensity; AT – time to ascent; LT – time to lighten.

PIT, AT, and LT in IPTL in a normal liver parenchyma were 10.16 ±1.76 s, 29.18 ±9.99 s, 18.30 ±6.67 s, and 79.00 ±16.87 s, respectively.

Comparison of ET, PIT, AT, and LT among IPTL, VX2 tumors and a normal liver

The ET, PIT and LT in VX2 tumors were significantly shorter than those of IPTL and a normal liver (IPTL and VX2 tumors, p-value in ET group (P_{ET}) = 0.000, p-value in PIT group (P_{PIT}) = 0.011, p-value in AT group (P_{AT}) = 0.984, p-value in LT group (P_{LT}) = 0.000; normal liver and VX2 tumors, $P_{ET} = 0.000$, $P_{PIT} = 0.025$, $P_{AT} = 0.146$, $P_{LT} = 0.000$). There was no significant difference for ET, PIT, AT, and LT between IPTL and a normal liver ($P_{ET} = 0.888$, $P_{PIT} = 0.658$, $P_{AT} = 0.152$, $P_{LT} = 0.645$) (Table 4).

Discussion

An ultrasound examination is usually the first line of investigation in the assessment of liver disease because it is non-invasive and widely available. The detection of focal hepatic lesions is relatively straight-forward with sonography, but the differentiation between benign and malignant lesions is usually difficult. There are different blood supply patterns observed for different tumors; therefore, assessment of tumor perfusion and blood supply is very useful to differentiate between benign and malignant focal lesions of the liver. Knowledge of the vascularity of a hepatic mass is essential in determining the nature of the mass. To this end, CT and MRI are performed regularly with contrast agents using different methods of administration and different imaging sequences to optimize vascular information.[19] With the rapid development of contrast-enhanced ultrasound and time-intensity curve quantification software, low-MI gray-scale harmonic imaging has provided an effective technique to identify the focal liver lesions[20–22] because low-MI continuous harmonic imaging without destroying the contrast bubbles reveals vessels that are not seen when conventional Doppler US modes are used.

Inflammatory pseudotumor of the liver is a relatively benign tumor-like lesion. It was originally described in the lung.[23] The liver is the 2nd most common site.[24] The prognosis for IPTL is good and spontaneous regression has been described.[8] The knowledge of IPTL is limited because of the small number of reported cases. With surgery and imaging techniques for advanced cases, more and more IPTL cases were reported.[4,7,9] Inflammatory pseudotumor of the liver is classified into 3 subtypes according to its pathological features: hyalinized sclerosing granuloma, xanthogranuloma and plasma cell granuloma.[6,25] This classification is reflected in a variety of radiological findings that have been reported. Inflammatory pseudotumor of the liver is often misdiagnosed as a malignant tumor based on the imaging findings. Therefore, improving knowledge about IPTL imaging is important to avoid unnecessary invasive therapy. To date, reports about IPTL are mostly clinical cases and there is an absence of reliable animal model for experimental research. There is a report[16] that injecting FCA into the liver can induce IPTL lesions. However, when FCA was injected directly into the lobe of livers of 10 rabbits, histopathological examination proved that no focal lesions formed instead of large size areas with diffuse necrosis. The reason for this is the solution flowed along the parenchyma and it was difficult to form focal nodule in situ. Then, we modified the method and inserted 1 mm^3 of gelfoam first into the left and right liver lobe with ophthalmic forceps through incisions at laparotomy. Because FCA is liquid and easy to flow, the gelfoam can restrict the flow of injected FCA and form nodules. Freund's complete adjuvant contains tuberculin, abundant steroid, protein, and polysaccharide, which can induce damage, degeneration and necrosis of hepatic cells. At the same time, fibrous tissue proliferated because of inflammatory cell

infiltration. The histopathological examination in our experiment proved that the modified method could establish the IPTL animal model successfully, and after implanting of 20 lesions, 17 nodules were formed successfully (85%).

Inflammatory pseudotumor of the liver is a proliferating fibrovascular lesion pathologically characterized by infiltrated chronic inflammatory cells including lymphocytes, histiocytes and plasma cells.[26] The microscopical results in our modified IPTL model revealed proliferated granulomas with marked fibrous tissue infiltrated by a mixed population of inflammatory and multinucleate cells. Degenerated liver tissue was seen in the center of the nodule. Scattered necrosis, diffused fat and amorphous substance were also present. Inflammatory reaction and fibrous tissue were observed at the periphery of the lesions. More venous vessels were seen in arteries in the peripheral zone of the lesion; degeneration and necrosis were seen in most of the tiny arteries. It was proved that the modified IPTL model is a proliferated nodule, which mostly supplied by portal vein, short of hepatic artery supply.

VX2 hepatic tumor is an established malignant model in rabbits.[27] It has the similar blood supply as human malignant tumor which is supplied mainly by artery vessels. The IPTL is supplied mainly by venous vessels same as the normal live parenchyma. The various hemodynamic changes result in a variety of enhancements in their IPTL imaging, normal liver, surrounding parenchyma, and VX2 tumor. The experiment results showed that the IPTL had similar patterns as the normal liver and the surrounding parenchyma because of the same blood supply of venous vessels. No significant difference was observed in ET, PIT, AT, and LT between the IPTL and normal liver and surrounding parenchyma. However, VX2 tumor showed a rapid wash-in/wash-out of enhancement because the supply is mainly by arteries. The ET, PIT and LT in VX2 tumors were observed significantly earlier than those of IPTL. The ET, PIT, AT, and LT in VX2 tumors were observed significantly earlier than those of the normal liver and surrounding parenchyma. This prominent difference of enhancement combined with the time-intensity curve quantification improves the accuracy of diagnosis. Contrast-enhanced sonography improves sensitivity and specificity in discriminating between benign and malignant focal liver lesions compared with baseline sonography.

The enhanced features in our IPTL model differ from that of the clinical report, in which the enhanced IPTL was similar to HCC.[28] The different pathological features might result in a diversity of enhanced imaging. A pilot study about the proliferated nodule short of hepatic artery supply was performed as a part of this study. The pathology of this model might be different than in the reported clinical case, in which inflammatory cell infiltration might be the main feature. Thus, further studies, e.g., related to the different growth stages and different pathology foundations of IPTL, need to be undertaken.

Conclusions

The study established a modified IPTL model in rabbits. The modified model easily formed solitary and solid lesion in situ, and had the advantages of high incidence rate, short latent period and easiness in duplication. Inflammatory pseudotumor of the liver is mainly supplied by the same vein as normal living tissue, and a small part of blood supply is provided by hepatic artery.

Based on the preliminary data, we believe that the low-MI continuous gray-scale harmonic contrast-enhanced ultrasound and analysis of wash-in/wash-out curves can be useful and reliable in diagnosing liver focal lesions and would be potentially useful in a clinical setting. However, our study is still in its early stages and is based on a small number of cases; therefore, further research needs to be performed.

ORCID iDs

Ying Shi https://orcid.org/0000-0002-5061-7119
Xinghua Wang https://orcid.org/0000-0001-9586-5573
Yingyan Qiao https://orcid.org/0000-0002-7910-4210
Xueping Bai https://orcid.org/0000-0002-2622-178X
Qinxiu Wang https://orcid.org/0000-0002-6676-4092
Chenggong Lei https://orcid.org/0000-0002-3714-5102

References

1. Pack GT, Baker HW. Total right hepatic lobectomy: Report of a case. *Ann Surg*. 1953;138(2):253–258.
2. Nitta T, Kataoka J, Inoue Y, et al. A case of multiple inflammatory hepatic pseudotumor protruding from the liver surface after colonic cancer. *Int J Surg Case Rep*. 2017;37:261–264.
3. Al-Jabri T, Sanjay P, Shaikh I, Woodward A. Inflammatory myofibroblastic pseudotumor of the liver in association with gall stones: A rare case report and brief review. *Diagn Pathol*. 2010;5:53.
4. Yafei Z, Hongwei L, Hong J, Yiming L. Inflammatory pseudotumor of the liver: A case report and literature review. *Intractable Rare Dis Res*. 2015;4(3):155–158.
5. Fukuya T, Honda H, Matsumata T, et al. Diagnosis of inflammatory pseudotumor of the liver: Value of CT. *AJR Am J Roentgenol*. 1994; 163(5):1087–1091.
6. Honmyoa N, Kobayashia T, Tashiroa H, et al. Inflammatory pseudotumor of the liver occurring during the course of hepatitis C virus-related hepatocellular carcinoma treatment: A case report. *Int J Surg Case Rep*. 2016;20:96–100.
7. Gesualdo A, Tamburrano R, Gentile A, Giannini A, Palasciano G, Palmieri VO. A diagnosis of inflammatory pseudotumor of the liver by contrast-enhaced ultrasound and fine-needle biopsy: A case report. *Eur J Case Rep Intern Med*. 2017;4(2):000495.
8. Kawaguchi T, Mochizuki K, Kizu T, et al. Inflammatory pseudotumor of the liver and spleen diagnosed by percutaneous needle biopsy. *World J Gastroenterol*. 2012;18(1):90–95.
9. Yamaguchi J, Sakamoto Y, Sano T, Shimada K, Kosuge T. Spontaneous regression of inflammatory pseudotumor of the liver: Report of three cases. *Surg Today*. 2007;37(6):525–529.
10. Matsuo Y, Sato M, Shibata T, et al. Inflammatory pseudotumor of the liver diagnosed as metastatic liver tumor in a patient with a gastrointestinal stromal tumor of the rectum: Report of a case. *World J Surg Oncol*. 2014;12:140.
11. Leoni S, Serio I, Pecorelli A, Marinelli S, Bolondi L. Contrast-enhanced ultrasound in liver cancer. *Hepatic Oncol*. 2015;2(1):51–62.
12. Durot I, Wilson SR, Willmann JK. Contrast-enhanced ultrasound of malignant liver lesions. *Abdom Radiol (NY)*. 2018;43(4):819–847.
13. Derchi LE, Martinoli C, Pretolesi F, Crespi G, Buccicardi D. Quantitative analysis of contrast enhancement. *Eur Radiol*. 1999;9(Suppl 3): S372–376.

14. Marret H, Sauget S, Giraudeau B, et al. Contrast-enhanced sonography helps in discrimination of benign from malignant adnexal masses. *J Ultrasound Med*. 2004;23(12):1629–1639.
15. Kljucevsek D, Vidmar D, Urlep D, Dezman R. Dynamic contrast-enhanced ultrasound of the bowel wall with quantitative assessment of Crohn's disease activity in childhood. *Radiol Oncol*. 2016:50(4):347–354.
16. Li J, Dong BW, Yu XL, Li C. Ultrasonographic portography with low mechanical index gray-scale imaging in hepatic VX2 tumor. *Ultrasound Med Biol*. 2006;32(5):641–647.
17. Yang W, Mou S, Xu Y, Du J. Contrast-enhanced ultrasonography for assessment of tubular atrophy/interstitial fibrosis in immunoglobulin A nephropathy: A preliminary clinical study. *Abdom Radiol (NY)*. 2018;43(6):1423–1431.
18. Xu YK, Liu XY, Zhang JN, et al. Experiment study of intravenous hepatosplenography with a new iodized oily emulsion for detection of small liver foci: Preliminary results. *MMI Bimonthly*. 1998;7:272–273.
19. Caramella T, Novellas S, Fournol M, et al. Imaging of inflammatory pseudotumors of the liver [in French]. *J Radiol*. 2007;88(6):882–888.
20. Lee J, Jeong WK, Lim HK, Kim AY. Focal nodular hyperplasia of the liver: Contrast-enhanced ultrasonographic features with sonazoid. *J Ultrasound Med*. 2018;37(6):1473–1480.
21. Soye JA, Mullan CP, Porter S, Beattie H, Barltrop AH, Nelson WM. The use of contrast-enhanced ultrasound in the characterisation of focal liver lesions. *Ulster Med J*. 2007;76(1):22–25.
22. Bagley JE, Paul DE, Halferty S, DiGiacinto D. The use of contrast-enhanced ultrasonography for the characterisation of focal liver lesions. *Sonography*. 2018;5(3):120–134.
23. Vjjanic GM, Milovanovic D, Aleksandrovic S. Aggressive inflammatory pseudotumor of the abdomen 9 years after therapy for Wilms tumor: A complication, coincidence, or association. *Cancer*. 1992;70(9): 2362–2366.
24. Toda K, Yasuda I, Nishigaki Y, et al. Inflammatory pseudotumor of the liver with primary sclerosing cholangitis. *J Gastoenterol*. 2000;35(4): 304–309.
25. Milias K, Madhavan KK, Bellamy C, Garden OJ, Parks RW. Inflammatory pseudotumors of the liver: Experience of a specialist surgical unit. *J Gastroenterol Hepatol*. 2009;24(9):1562–1566.
26. Oto T, Akata D, Besim A. Peritoneal inflammatory myofibroblastic pseudotumor metastatic to the liver: CT findings. *Eur Radiol*. 2000; 10(9):1501.
27. Mastuda H, Sugimachi K, Kuwano H, Mori M. Hyperthermia, tissue microcirculation, and temporarily increased thermosensitivity in VX2 carcinoma in rabbit liver. *Cancer Res*. 1989;49(10):2777–2782.
28. Wang Y, Yu XL, Cheng ZG. Contrast-enhanced ultrasonographic features of inflammatory pseudotumor of the liver. *Chin J Med Ultrasound*. 2006;3:31–33.